Study of the Losses in Fluid Machinery with the Help of Entropy

Martin Böhle, Annika Fleder, Matthias Mohr

Study of the Losses in Fluid Machinery with the Help of Entropy

Martin Böhle[1], Annika Fleder[1], Matthias Mohr [1]*

ISROMAC 2016

International Symposium on Transport Phenomena and Dynamics of Rotating Machinery

Hawaii, Honolulu

April 10-15, 2016

Abstract

In the current design process of turbomachinery the use of CFD methods is state of the art. With CFD calculations we are able to predict the performance characteristics of the machines. In most of the cases the machines are rated based on their performance alone. A detailed evaluation of the losses involved often is not conducted, mainly because there is no established method to analyze the location and mechanisms of loss production. This leads to the fact that the loss mechanisms for some turbo machines are not known in detail, although they are very important to completely understand the operation principle of the machines and have a huge influence on their performance. If the location and quantity of losses were known, it would be possible to perform a selective optimization of the machine. The question is just how to calculate and localize the losses and evaluate them with CFD. In his thesis Kock introduces a method, to identify losses in CFD. His method is based on the entropy production rates in turbulent flow fields. In this paper the method is applied on hydraulic fluid machinery and two different machine types are discussed in detail. Those are a side channel pump and an inducer. The locations of the losses are detected and the size of losses will be evaluated by applying the method of Kock.

[1] *Institute of Fluid Mechanics and Fluid Machinery, Department of Mechanical Engineering, Technical University of Kaiserslautern, Germany*

*__Corresponding author__: matthias.mohr@mv.uni-kl.de

INTRODUCTION

In all fluid machinery there exist different kind of losses. We have to differentiate between internal losses and external losses. The external losses are, for example, losses in bearings, gears and shaft seals. Those losses are not included in the CFD calculation whereas the internal losses are considered by CFD. Among the latter are shock losses and friction losses. The different types of internal losses can be summarized in dissipation.

The numerical simulation offers the opportunity to calculate the flow in the machines spatially and temporally dependent. Thus the flow in the machines can be observed three dimensionally at an arbitrary point in time. The calculated quantities are the fields of pressure, temperature and velocity. Derived quantities like pressure coefficient and efficiency can be calculated directly during post processing. To identify the different internal losses Herwig and Kock [1, 2, 3] proposed a direct method based on the evaluation of entropy production in turbulent flow fields. The advantage of the method is that it can be applied to a CFD simulation in a pure postprocessing step. The content of the present paper is the application of this method to two examples of hydraulic turbomachinery, a side channel pump and an inducer. For those two types of machines numerical investigations are conducted. To assess the quality of the numerical results they are compared to available experimental data. Eventually a detailed analysis of the losses based on the numerical data is performed and the influence of the turbulence model is examined.

1. METHODS

With the help of CFD it is possible to calculate the time-dependent flow field in all kind of turbomachinery. The governing equations that are solved to describe the flow are the equations of conservation of mass, conservation of momentum and conservation of energy. The basis of the energy equation calculated in CFD is the first law of thermodynamics. Herwig and Kock use the production of entropy as a direct parameter for the efficiency of a technical system [3]. In the transport equation of entropy heat transfer and pressure drop are linked to one quantity. They describe two methods to calculate the entropy production in the context of a CFD simulation process. In this paper the so called direct method will be considered. One main feature of the direct method is that the entropy is treated as a postprocessing quantity. In the cases of hydraulic fluid machinery, the fluid is commonly regarded as incompressible and the heat transfer is negligibly. Therefore

the energy equation is not calculated.

The specific entropy s is a state variable that, according to the second law of thermodynamics, grows in every real and thus irreversible technical process. Its transport or balance equation is given in the literature (e.g. [4] or [5]) and can be written as follows:

$$\rho\left(\frac{\delta s}{\delta t}+u\cdot\frac{\delta s}{\delta x}+v\cdot\frac{\delta s}{\delta y}+w\cdot\frac{\delta s}{\delta z}\right) = -\mathrm{div}\left(\frac{\vec{q}}{T}\right)+\frac{\Phi}{T}+\frac{\Phi_\theta}{T^2} \tag{1}$$

The first term on the right-hand side of equation (1) describes the reversible heat transfer $\mathrm{div}\left(\frac{\vec{q}}{T}\right)=\mathrm{div}\left(-\frac{\lambda}{T}\,\mathrm{grad}\,T\right)$. This term is not important for the calculation of the losses. The function $\frac{\Phi}{T}$ describes the irreversible part produced by friction, and $\frac{\Phi_\theta}{T^2}=-\frac{\vec{q}}{T^2}\mathrm{grad}\,T$ the irreversible part produced by heat transfer. This means that in those two terms describing the irreversible part of entropy production all losses that occur in a machine by friction and heat transfer are included. As mentioned before, the heat transfer is negligible for the pumps under examination.

The terms $\frac{\Phi}{T}$ and $-\frac{\vec{q}}{T^2}\mathrm{grad}\,T$ are always greater than zero because in an adiabatic system with $\vec{q}=0$ the entropy cannot decrease. In industrial applications of CFD analysis of turbomachinery usually the time-averaged Navier-Stokes (RANS) equations are solved. Denoting the time averaged quantities by an overbar, the time-averaged version of the transport equation for entropy, as shown in [1], can be written in the following form:

$$\begin{aligned}\rho\left(\frac{\delta\bar{s}}{\delta t}+\bar{u}\cdot\frac{\delta\bar{s}}{\delta x}+\bar{v}\cdot\frac{\delta\bar{s}}{\delta y}+\bar{w}\cdot\frac{\delta\bar{s}}{\delta z}\right)\\ =\overline{-\mathrm{div}\left(\frac{\vec{q}}{T}\right)}-\rho\left(\overline{\frac{\delta u's'}{\delta x}}+\overline{\frac{\delta v's'}{\delta y}}+\overline{\frac{\delta w's'}{\delta z}}\right)\\ +\overline{\left(\frac{\Phi}{T}\right)}+\overline{\left(\frac{\Phi_\theta}{T^2}\right)}\end{aligned} \tag{2}$$

Important for our studies is the term of entropy production caused by dissipation $\overline{\left(\frac{\Phi}{T}\right)}$. This term is composed as follows:

$$\overline{\left(\frac{\Phi}{T}\right)}=\dot{S}^{\bar{D}}_{pro}+\dot{S}^{D'}_{pro} \tag{3}$$

The first term on the right-hand side of equation (3) stands for the entropy production by viscous or direct dissipation. It can be calculated directly in the CFD postprocessing procedure by using the following equation:

$$\begin{aligned}\dot{S}^{\bar{D}}_{pro}=\frac{\mu}{\bar{T}}\Bigg[2\cdot\left[\left(\frac{\partial\bar{u}}{\partial x}\right)^2+\left(\frac{\partial\bar{v}}{\partial y}\right)^2+\left(\frac{\partial\bar{w}}{\partial z}\right)^2\right]+\\ \left(\frac{\partial\bar{v}}{\partial x}+\frac{\partial\bar{u}}{\partial y}\right)^2+\left(\frac{\partial\bar{w}}{\partial y}+\frac{\partial\bar{v}}{\partial z}\right)^2+\left(\frac{\partial\bar{u}}{\partial z}+\frac{\partial\bar{w}}{\partial x}\right)^2\Bigg]\end{aligned} \tag{4}$$

The second term on the right-hand side of equation (3) describes the entropy production by turbulent dissipation which is also called indirect dissipation. It can be expressed as follows:

$$\begin{aligned}\dot{S}^{D'}_{pro}=\frac{\mu}{\bar{T}}\Bigg[2\cdot\left[\left(\frac{\partial u'}{\partial x}\right)^2+\left(\frac{\partial v'}{\partial y}\right)^2+\left(\frac{\partial w'}{\partial z}\right)^2\right]+\\ \left(\frac{\partial v'}{\partial x}+\frac{\partial u'}{\partial y}\right)^2+\left(\frac{\partial w'}{\partial y}+\frac{\partial v'}{\partial z}\right)^2+\left(\frac{\partial u'}{\partial z}+\frac{\partial w'}{\partial x}\right)^2\Bigg]\end{aligned} \tag{5}$$

This expression can't be computed directly, because the fluctuating quantities are not available in the CFD solution based on the RANS equations. To circumvent this problem the following model equation is proposed by Kock [1, 2]:

$$\dot{S}^{D'}_{pro}=\frac{\rho\epsilon}{\bar{T}} \tag{6}$$

It uses the dissipation rate of turbulent kinetic energy ϵ which is provided by the turbulence model and is readily available during postprocessing.

We have to consider that within this approach errors are introduced by the turbulence model itself which - as its name implies - is just a model and by the approximation involved in the formulation of model equation (6).

Following Kock [6] the entropy production rates caused by viscous and turbulent effects (equations (4)-(6)) are connected to the viscous and turbulent dissipation respectively through the relations:

$$\Phi_{\bar{D}}=\bar{T}\,\dot{S}^{\bar{D}}_{pro} \tag{7}$$

$$\Phi_{D'}=\bar{T}\,\dot{S}^{D'}_{pro} \tag{8}$$

Finally the dissipation portions $\Phi_{\bar{D}}$ and $\Phi_{D'}$ can be used to calculate the corresponding power losses by integrating over the volume of interest:

$$P_{\bar{D}}=\int_V\Phi_{\bar{D}}dV=\int_V\bar{T}\,\dot{S}^{\bar{D}}_{pro}dV \tag{9}$$

$$P_{D'}=\int_V\Phi_{D'}dV=\int_V\bar{T}\,\dot{S}^{D'}_{pro}dV \tag{10}$$

The calculation of the turbulent dissipation depends on the turbulence model. In the case of the side channel pump three different turbulence models, the k-ϵ model, the k-ω and the k-ω-SST model are used and their influence on the turbulent dissipation is shown. In the case of the inducer only the k-ω-SST model is utilized. For the remainder of the current paper we refer to the three applied models as k-ϵ, k-ω and SST respectively.

As will be seen later the viscous dissipation is small compared to the turbulent dissipation in the case of the examined machines. Hence to investigate the loss mechanisms and locations of loss production it is helpful to visualize the spatial distribution of turbulent dissipation inside of the machine. For this purpose we introduce the dimensionless loss coefficient $\zeta_{D'}$. The loss coefficient is defined in the following equation:

$$\zeta_{D'}=\frac{\Phi_{D'}\cdot d_a}{\omega^2\cdot\rho\cdot\dot{V}} \tag{11}$$

The loss coefficient depends on the volume flow rate $\dot{V}$, the outer diameter of the impeller d_a, the angular velocity ω and the turbulent dissipation $\Phi_{D'}$. It can therefore be used to compare different operation points and machines.

2. APPLICATION 1: SIDE CHANNEL PUMP

2.1 Numerical set-up

In Figure 1 the simulation model of the side channel pump is depicted. It consists of three computational domains. Those are the inlet tube colored in grey, the impeller colored in red and the side channel including the outlet tube colored in grey. The domains are discretized with hexahedral multiblock grids that were created using ANSYS ICEM CFD. The computations are performed with the commercial CFD code ANSYS CFX 14.5. Between the inlet tube and the impeller and between the impeller and the side channel transient rotor-stator interfaces are used (Figure 1). At the inflow the average total pressure is prescribed. The outlet boundary condition is realized as a velocity opening to prevent walls in the outlet caused by backflow of the fluid, which is generated by the strong swirl in the outlet tube of the pump. The default algorithm of velocity-pressure coupling, implemented in CFX, is applied. We use a time step of 0.0001 s to simulate the pump at a speed of 1500 min^{-1}. For each operation point at least two full impeller turns are simulated to ensure periodic converged solutions. Pressure, momentum and velocities have to be time averaged over the pulsation length due to the characteristic pulsations of side channel pumps. The pulsation length is calculated as $360/z$. To evaluate the influence of the turbulence model on the losses, the numerical calculations are carried out with three different turbulence models as already mentioned above.

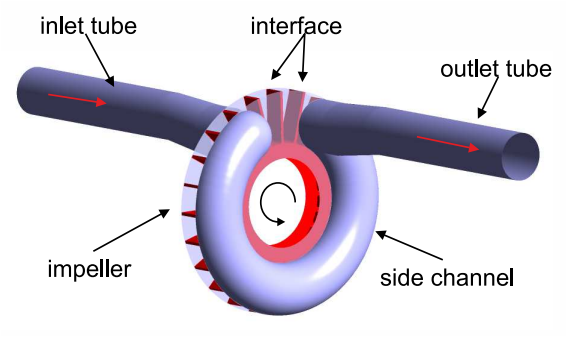

Figure 1. Simulation set-up of the side channel pump

2.2 Influence of the turbulence model on the performance

Three different operation points (part load, BEP, over load) are calculated with the the k-ω-SST model, with the k-ϵ model and with the k-ω model. The numerical results are compared with the performance data obtained by measurements at the test facilities of the TU Kaiserslautern. Of particular interest is the influence of the turbulence model on pressure coefficient and shaft power and thus on the efficiency. Additionally the influence of the turbulence model on the dissipation power of the impeller and the side channel is examined.
Figure 2 shows the pressure coefficient for the different turbulence models in comparison to measurements. Obviously the

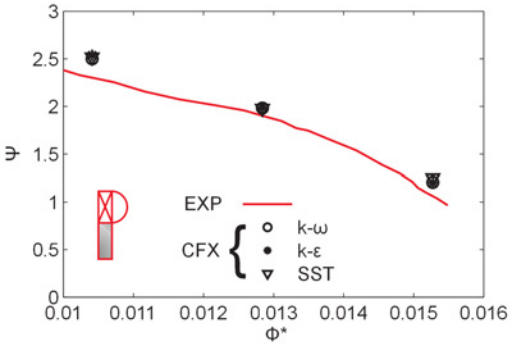

Figure 2. Pressure coefficient for the different turbulence models compared to experimental data

influence of the turbulence model on the calculated pressure coefficients is very small for all simulations. The pressure coefficients are almost identical in each operation point.

The influence of the turbulence model on the efficiency is larger as can be seen in figure 3. The best efficiency is calculated with the k-ω-SST model. Compared to the lowest efficiency that is calculated with the k-ϵ model there is a difference of about 2 %. In the measured efficiency mechanical losses of the bearings and the sealing are included. Because these external losses cannot be considered in the CFD simulations the measured efficiency curve lies below the numerically calculated points.

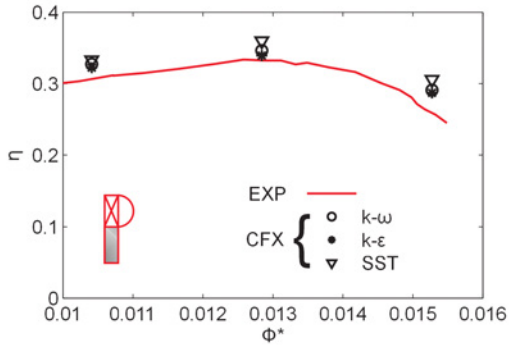

Figure 3. Efficiency for the different turbulence models compared to experimental data

2.3 Dissipation Power and loss analysis

The occurring losses will be examined with the help of the dissipation power. As already discussed we have to distinguish between the power losses due to viscous dissipation ($P_{\bar{D}}$) and the losses due to turbulent dissipation ($P_{D'}$).
Figure 4 shows the dissipation power loss, averaged over one pressure pulsation, for the side channel domain (index SK) and

the impeller domain (index LR) measured in watt. The viscous dissipation power is a lot smaller in all operation points than the turbulent dissipation power. Their trend is the same. The analytically undetermined losses (inlet shock of the main and the circulating flow, friction and gap losses) decrease with increasing volume flow rate. Shock and gap losses are included in the dissipation power of the impeller, that decreases with increasing volume flow. The viscous and turbulent dissipation power in the side channel increase slightly. The losses in the side channel are mainly friction losses. Those increase with increasing volume flow rate and and the associated higher flow velocities in the side channel. The losses in the inlet tube are small and are neglected in the figure.

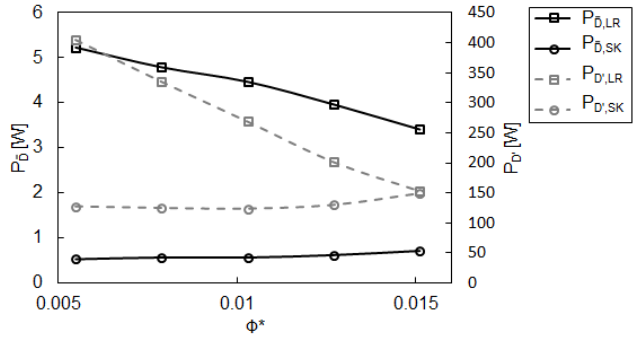

Figure 4. Dissipation power for different volume flow rates for the impeller and the side channel

Figure 5 depicts three views of the model of the side channel pump calculated in the BEP at the maximum point of pulsation. In the figure impeller and side channel are displayed three times side by side each with a coaxial plane. Viewed from left to right, the planes are located at an outer, a middle and an inner radius of the side channel. While the left and right view show vectors on the coaxial plane, the one in the center shows the streamlines to emphasize the circulating flow inside the blade channel. In addition, a contour plot of the loss coefficient $\zeta_{D'}$ is displayed on all of the coaxial planes. The $\zeta_{D'}$ values are 0 for the free flow in the side channel and about 12, where the losses are particularly high. An isosurface with $\zeta_{D'} = 12$ is shown for each simulation configuration. The isosurface is especially developed in the outlet and in the inlet region (no. 3 in figure 5). In those regions the losses are large. They are induced by eddies, as can be seen from the vectors and streamlines on the section planes. In the left view the plane is located at an outer radius. At this radius the fluid exits from the impeller into the side channel with small values of $\zeta_{D'}$. Only at the blade surfaces and between the impeller and side channel walls friction losses can be clearly recognized (no. 2 in figure 5). At the middle and lower radii illustrated in the two subsequent views, the fluid enters into the impeller with notable shock losses at the blade edges. These are indicated with no. 1 in figure 5. Inside the impeller regions with higher losses are situated. Due to the large difference between flow angle and blade angle flow separation occurs inside the impeller resulting in the development of vortices. Those are responsible for the increase of losses. Figure 6 depicts the turbulent dissipation power in the impeller, figure 7 shows the turbulent dissipation power in the side channel. For the impeller as well as for the side channel the k-ϵ model predicts the highest dissipation power. The smallest losses are obtained when using the k-ω-SST model. This behavior is consistent to the efficiency characteristics of the pump obtained with the three different turbulence models and shown in figure 3. In general, the losses in the impeller decrease with increasing volume flow rate and the losses in the side channel increase with increasing volume flow rate. This is valid for all volume flows and turbulence models except for the simulation at overload with the k-ϵ model. While the losses in the impeller coincide quite well in case of the simulations using the k-ω and the k-ϵ model, the losses in the side channel agree better for the k-ω and k-ω-SST model. Using the k-ϵ model results by far in the highest losses in this region. To

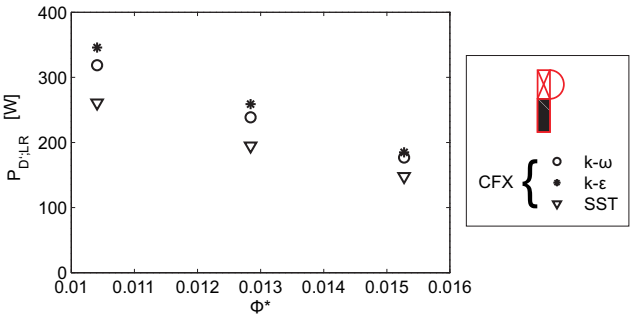

Figure 6. Turbulent dissipation power in the impeller for the different turbulence models

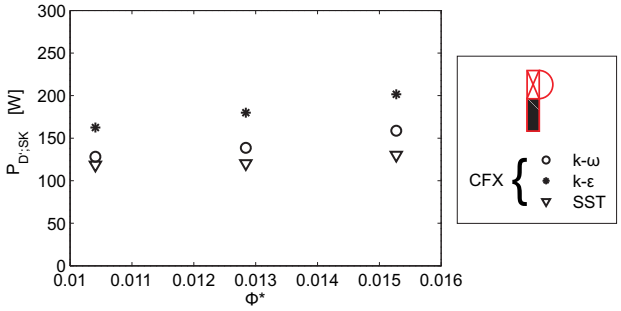

Figure 7. Turbulent dissipation power in the side channel for the different turbulence models

determine the locations where the highest losses occur and why losses are in general higher inside the impeller than in the side channel we investigate the loss coefficient ζ'_D for the different turbulence models on different cut sections through the inside of the pump. Figures 9, 10 and 11 each show the distribution of ζ'_D at the highest pressure amplitude in the pumps BEP. The distribution of the coefficient looks similar in all cases. The highest losses are situated in the inlet, the interrupter and the outlet region and tend to be located at the inner radii. These regions correspond to the regions of strong

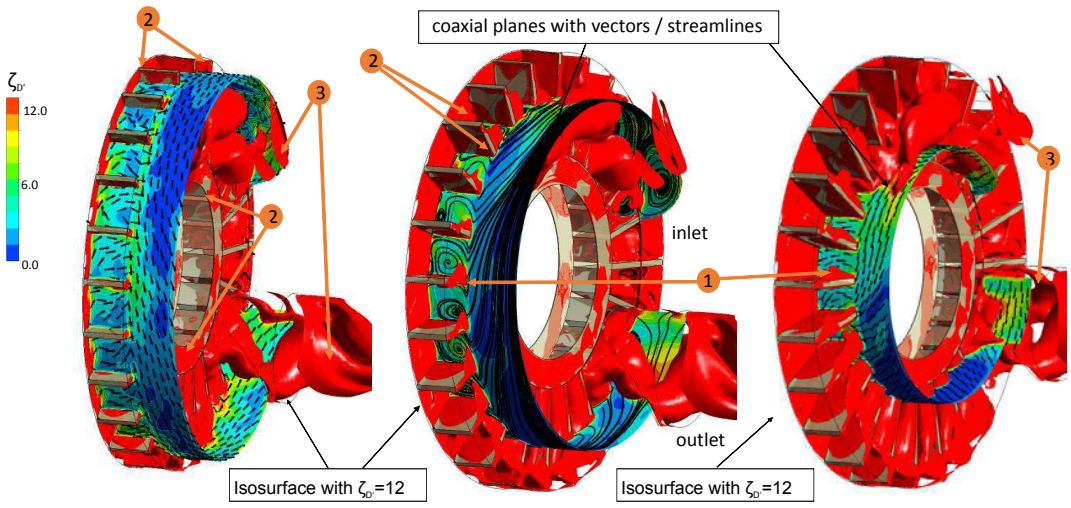

Figure 5. Losses in the side channel pump

flow separation and vortices. The k-ω-SST model predicts the smallest areas containing the highest loss coefficient. Figure 10 shows the distribution of the loss coefficient on a plane in the middle of the gap between impeller and casing for all three turbulence models. The maximum loss coefficients found on this plane are substantially higher than in the middle of the impeller. Compared to figure 9 with a maximum loss coefficient of 30, values up to $\zeta_{D'} = 100$ can be found here. The distribution of the loss coefficient again is quite similar for all the considered cases. In the regions of high velocities and thus high friction the highest values of loss coefficient can be observed. Figure 8 depicts the loss coefficient in the

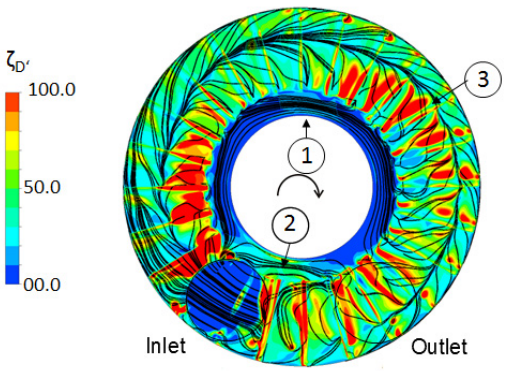

Figure 8. Loss coefficient and streamlines calculated with k-ω-SST turbulence model in the middle of the gap between impeller and side channel

case of the k-ω-SST model with additional streamlines on the plane in the middle of the gap. This allows us to observe the flow phenomena in the regions of high and low losses. The zones of convergent streamlines generally coincide with zones of lower losses independently of the applied turbulence model (see no. 3 in figure 8). Because of lower velocities in the backflow region the loss coefficients in the inner annular gap are also smaller (see no. 1 in figure 8). Higher losses occur in the annular gap near the interrupter. In this region higher velocities are caused by the large pressure gradient between suction- und discharge side of the pump (see no. 2 in figure 8).

From figure 11 it can be seen that independently of the used turbulence model there exist higher losses in the inlet and outlet regions while the overall distribution of the loss coefficient again looks roughly similar in all cases. In these regions the circulation of flow is not fully developed. Slightly increased losses can also be observed at the rotation axis of the circulating flow in the blade passages. The k-ϵ and k-ω model predict regions with somewhat higher losses compared to the result obtained using the k-ω-SST model.

At the wall of the side channel, shown in figure 12, we observe the largest differences between the turbulence models with respect to the calculated loss coefficient. Application of the k-ϵ model yields considerably higher losses compared to the other models. While for the k-ω and the k-ω-SST model large values of the loss coefficient are found only in the inlet region the k-ϵ model indicates high losses approximately along the first 45° of the side channel. In contrary to the other models the k-ϵ model predicts an additional region of higher losses near the outlet.

3. APPLICATION 2: INDUCER

3.1 Numerical set-up

As a second test case we consider a simple three-bladed helical inducer with axial hub shape under non-cavitating conditions. Steady state simulations of a periodical segment containing one blade passage of the inducer are performed using the commercial CFD code ANSYS CFX 15.0. Figure 13 shows the simulation setup consisting of three domains that represent the inlet pipe (blue), the inducer (grey) and the outlet pipe (blue). All domains are discretized with hexahedral elements only. To generate the grid for the inflow domain that includes the hub nose we used the software ANSYS ICEM

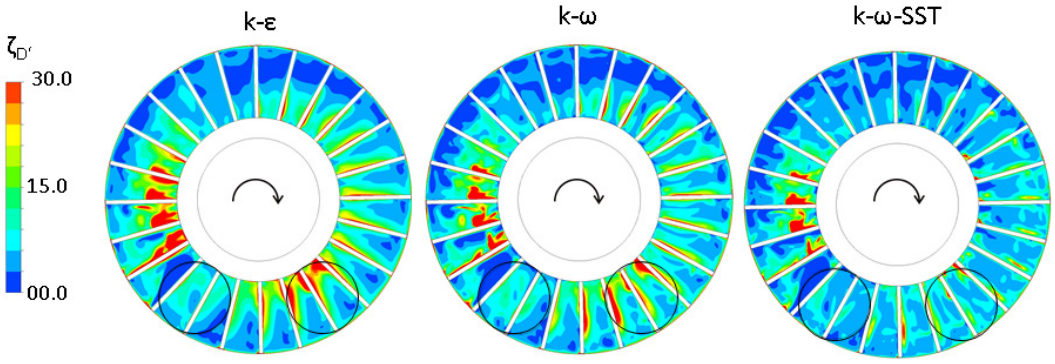

Figure 9. Loss coefficient in the middle of the impeller

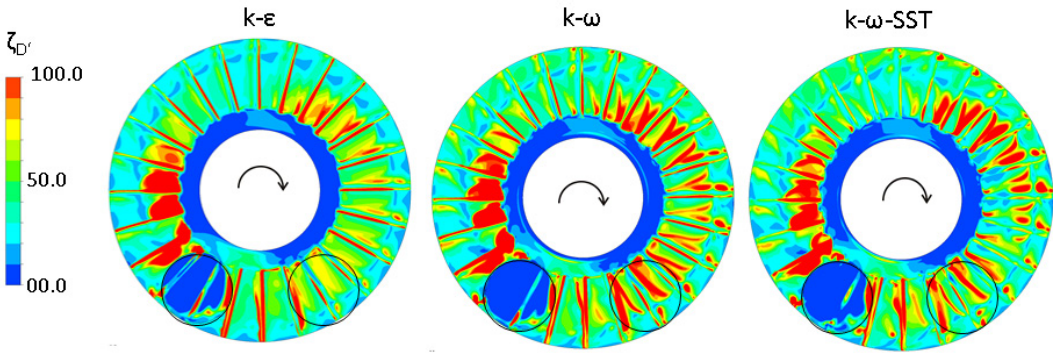

Figure 10. Loss coefficient in the gap between impeller and casing

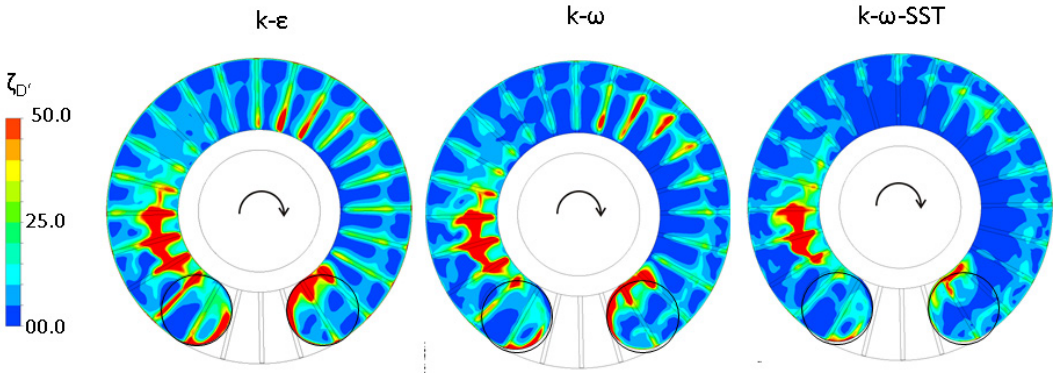

Figure 11. Loss coefficient in the plane of the exchange mass flow

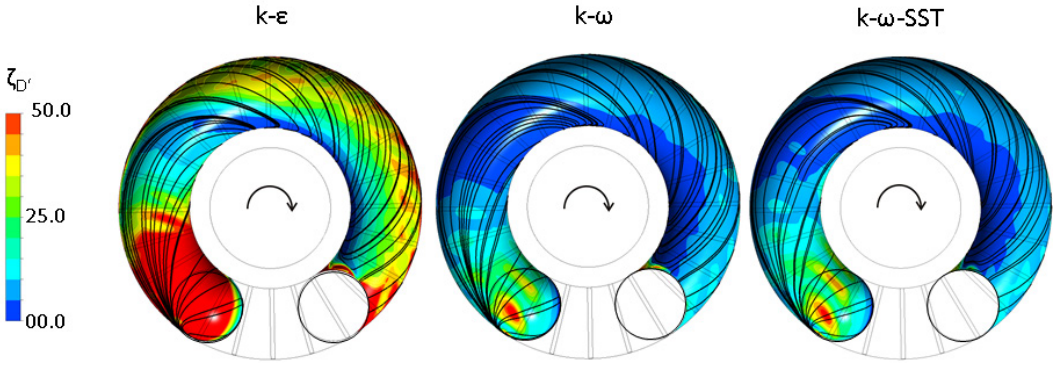

Figure 12. Loss coefficient on the wall of the side channel

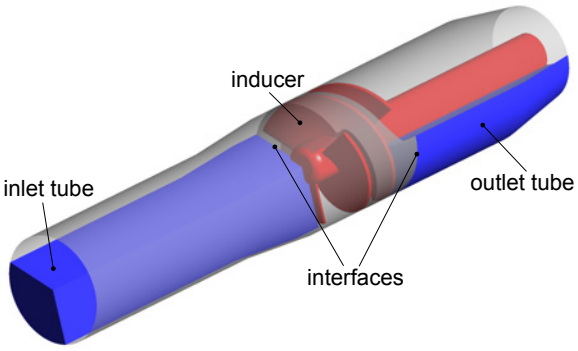

Figure 13. Simulation set-up of the inducer

CFD. The grids for the blade passage and the outlet domain were generated using ANSYS TurboGrid. To include the tip clearance losses in our numerical investigation we placed 25 cells in the gap between blade tip and shroud. The rotating domain containing the inducer is connected to the stationary inflow and outflow domains with frozen rotor interfaces. At the inlet boundary we prescribe the total pressure, at the outlet the mass flow is specified. We simulate five different volume flows at a speed of 3000 min^{-1}. As mentioned before we only use the k-ω-SST turbulence model for this case.

Figures 14 and 15 show the simulated data points in comparison to experimental results obtained at the test facilities of the TU Kaiserslautern. While a very good agreement exists for the pressure coefficient the numerically calculated efficiencies are throughout higher than the measured ones due to the mechanical losses that are not included in the CFD simulations. Especially under over-load conditions the efficiency is overpredicted by CFD. Figure 16 depicts the

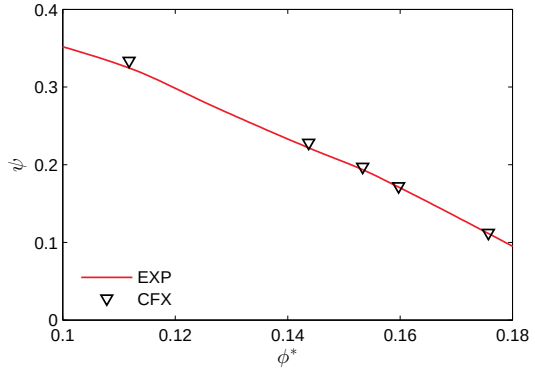

Figure 14. Measured and simulated pressure coefficient of the inducer

progression of the power losses as sums over all the simulation domains within the simulated operation range. While the power losses caused by viscous dissipation remain nearly constant a notable increase of the losses caused by turbulent dissipation occurs towards part-load. Like in the previous case of the side channel pump (see figure 4) the losses due to viscous dissipation are substantially smaller than the losses

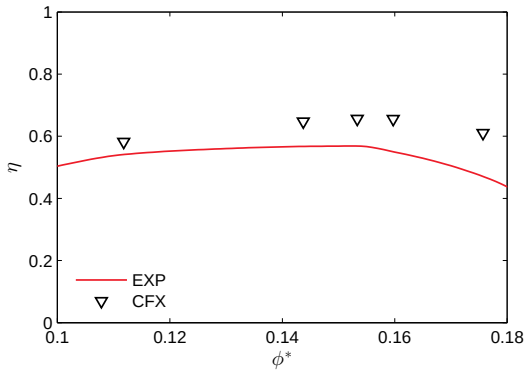

Figure 15. Measured and simulated efficiency of the inducer

due to turbulent dissipation although the discrepancy between the two loss types is not that large in the case of the inducer. Interestingly the magnitude of power losses caused by viscous dissipation are comparable in both applications whereas the inducer shows an overall lower level of losses due to turbulent dissipation. This is also confirmed by lower values of loss

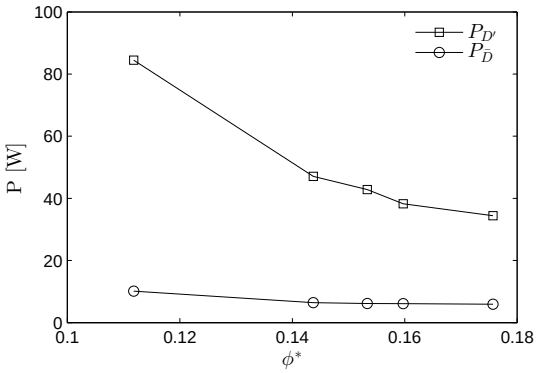

Figure 16. Dissipation power for different volume flow rates

coefficient $\zeta_{D'}$ throughout all the simulation domains. Figure 17 shows an isosurface for $\zeta_{D'} = 0.2$ and contours of the loss coefficient on cross sections of the blade passage at three axial stations for the simulation at the BEP. It should be noted that the color levels of the contour plots are scaled logarithmically to simultaneously cover the full range of loss coefficient and emphasize the significant regions. The cut section on the left is located close to the leading edge, the cut section on the right at the trailing edge and the third approximately halfway between the the two of them. As expected the largest losses occur at the outer diameters of the inducer blade and in the tip clearance where flow velocities and friction reach the highest values. The greatest losses can be observed at the blade tip close to the leading edge where the typical backflow vortex (no. 1 in figure 17) is generated. As can be seen from the isosurface in figure 17 broader regions of higher losses exist close to the blade surface near the leading edge and starting from the throat reaching along the suction surface down to the trailing edge of the inducer. Though not visible in the displayed figures

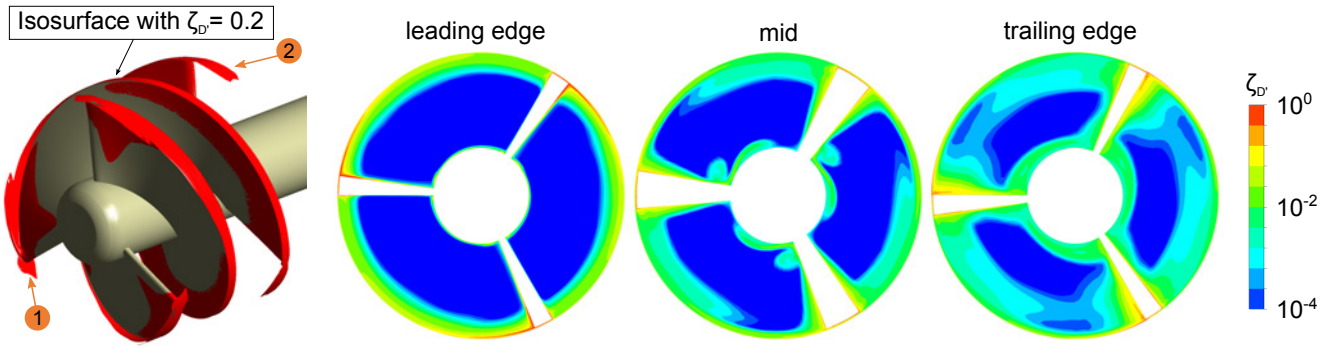

Figure 17. Isosurface and contours of loss coefficient $\zeta_{D'}$

a similar distribution of the loss coefficient can be found on the pressure surface. Downstream of the trailing edge a zone of losses near the shroud wall (no. 2 in figure 17) indicates the existence of a tip vortex. The contour plots on the cross sections depict the development of the loss distribution inside the blade passages from leading edge to trailing edge. Close to the leading ledge the core region of the flow is still almost undisturbed and thus shows low values of loss coefficient $\zeta_{D'}$. As already stated the loss coefficient increases with diameter and is especially high near the blade tip and along the shroud on the suction side of the blade. On the mid plane higher values of loss coefficient can be detected near the walls at the hub, blade and shroud that disturb the uniform distribution of loss coefficient in the core region. This indicates turbulent interaction of secondary flows with the core flow, causing an increase in losses. At the trailing edge position the core region containing small values of loss coefficient is further reduced and higher values can be found all over the hub and the blades.

4. DISCUSSION

In the first application, the side channel pump, we investigate the influence of the turbulence model on the predicted losses and their distributions. We can note that the occurrence of losses can be reasonably explained by all three turbulence models under examination. The higher losses in the impeller are due to the fact that the gap is included in this simulation domain and the complex flow pattern inside the impeller blade passages. Near the walls the k-ϵ model predicts, in general, higher values of loss coefficient than the other two models. The spatial distribution of the losses and the tendency of dissipation power to increase and decrease with changed operation conditions can be physically justified and qualitatively measured. As already indicated the absolute values of the local losses depend highly on the assumptions made by the turbulence model used. Therefore no statements regarding the correctness of the quantitative losses can be made. However the method applied in this paper can be understood as a simple tool to understand loss production processes and locate the regions that are critical for the development and improvement of turbomachinery by using CFD simulations.

Our second application deals with the flow through an inducer. We could observe similar trends of the power losses within the investigated operation range. The power losses caused by viscous dissipation are comparable and equally small for the side channel pump as well as for the inducer whereas the losses due to turbulent dissipation are lower in the case of the latter. This smaller amount of turbulent dissipation explains the better (but still low) efficiency of the inducer compared to the efficiency of the side channel pump. By visualization of the losses with the help of the loss coefficient we could identify and localize the flow features that are responsible for a large portion of dissipation. Furthermore the development of the distribution of the loss coefficient inside the blade passages could be observed with this postprocessing method. The insights gained into the structure of the losses can help to better understand the mechanisms involved in loss production and improve the design of the machines.

Concluding we can state that a qualitative analysis of the losses in turbomachinery can be performed with the simple postprocessing procedure demonstrated in the current work. The ability to detect critical flow regions regarding the production of losses creates the opportunity to selectively optimize existing geometry. However it should be remarked that the quantitative balance of powers could not be shown with the current method for the cases under examination. This issue needs further investigation and is part of our current research work.

ACKNOWLEDGMENTS

The simulations were conducted on the high performance cluster Elwetritsch at TU Kaiserslautern, which is part of the Alliance of High Performance Computing Rheinland-Pfalz (AHRP). We would like to thank for their kind support.

NOMENCLATURE

Latin symbols

Symbol	Description	Unit
$P_{\bar{D}}$	viscous dissipation power	W
$P_{\bar{D}'}$	turbulent dissipation power	W
V	volume	m^3
$\dot{V}$	volume flow	m^3/s
$\dot{S}^{\overline{D}}_{pro}$	entropy production rate by viscous dissipation per unit volume	W/Km^3
$\dot{S}^{D'}_{pro}$	entropy production rate by turbulent dissipation per unit volume	W/Km^3
T	temperature	K
d_a	outer diameter of the impeller	m
$\vec{q}$	heat flux density vector	W/m^2
s	specific entropy	J/(kgK)
t	time	s
u_a	circumferential velocity at d_a	m/s
u	velocity component in x-direction	m/s
v	velocity component in y-direction	m/s
w	velocity component in z-direction	m/s
x	x-coordinate	m
y	y-coordinate	m
z	z-coordinate	m

Greek symbols

Symbol	Description	Unit
Φ	dissipation	W/m^3
$\Phi_{\bar{D}}$	viscous dissipation	W/m^3
$\Phi_{D'}$	turbulent dissipation	W/m^3
Φ_θ	local dissipation by heat transfer	WK/m^3
ϵ	dissipation rate of turbulent kinetic energy per unit mass	m^2/s^3
$\zeta_{D'}$	loss coefficient	-
η	efficiency	-
μ	dynamic viscosity	kg/(ms)
ρ	density	kg/m^3
ϕ^*	flow coefficienct	-
ψ	pressure coefficient	-
ω	angular velocity	rad/s

Acronyms

BEP	best efficiency point
CFD	computational fluid dynamics
EXP	experiment
RANS	Reynolds-averaged Navier-Stokes

REFERENCES

[1] F. Kock and H. Herwig. Local entropy production in turbulent shear flows: a high-reynolds number model with wall functions. *International Journal of Heat and Mass Transfer*, 47:2205–2215, 2004.

[2] F. Kock and H. Herwig. Entropy production calculation for turbulent shear flows and their implementation in cfd codes. *International Journal of Heat and Fluid Flow*, 26:672–680, 2005.

[3] H. Herwig and F. Kock. Direct and indirect methods of calculating entropy generation rates in turbulent convective heat transfer problems. *International Journal of Heat and Mass Transfer*, 43:207–125, 2007.

[4] J. H. Spurk and N. Aksel. *Fluid Mechanics*. Springer-Verlag Berlin Heidelberg, 2008.

[5] H. Schlichting and K. Gersten. *Grenzschichttheorie*. Springer Verlag, 2006.

[6] F. Kock. *Bestimmung der lokalen Entropieproduktion in turbulenten Strömungen und deren Nutzung zur Bewertung konvektiver Transportprozesse*. PhD thesis, TU Hamburg-Harburg, Hamburg, 2003.